Solar Phys (2008) 252: 373–383
DOI 10.1007/s11207-008-9262-0

Three-Dimensional Reconstruction of Two Solar Coronal Mass Ejections Using the STEREO Spacecraft

Timothy A. Howard · S. James Tappin

Received: 27 June 2008 / Accepted: 20 August 2008 / Published online: 8 October 2008

Abstract Previous attempts to produce three-dimensional (3-D) reconstructions of coronal mass ejections (CMEs) have required either modeling efforts or comparisons with secondary associated eruptions near the solar surface. This is because coronagraphs are only able to produce sky-plane-projected images of CMEs and it has hence been impossible to overcome projection effects by using coronagraphs alone. The SECCHI suite aboard the twin STEREO spacecraft allows us to provide the means for 3-D reconstruction of CMEs directly from coronagraph measurements alone for the first time. We present these measurements from two CMEs observed in November 2007. By identifying common features observed simultaneously with the LASCO coronagraphs aboard SOHO and the COR coronagraphs aboard STEREO we have triangulated the source region of both CMEs. We present the geometrical analysis required for this triangulation and identify the location of the CME in solar-meridional, ecliptic, and Carrington coordinates. None of the two events were associated with an easily detectable solar surface eruption, so this triangulation technique is the only means by which the source location of these CMEs could be identified. We present evidence that both CMEs originated from the same magnetic structure on the Sun, but from a different magnetic field configuration. Our results reveal some insight into the evolution of the high corona magnetic field, including its behavior over time scales of a few days and its reconfiguration after a major eruption.

Keywords Corona · Coronal mass ejection · Three-dimensional geometry

1. Introduction

Solar coronal mass ejections (CMEs) are an important mechanism in the upper solar atmosphere, removing large amounts of energy and magnetic helicity from the Sun. They are

T.A. Howard (✉) · S.J. Tappin
Air Force Research Laboratory, National Solar Observatory, Sunspot, NM 88349, USA
e-mail: thoward@nso.edu

S.J. Tappin
e-mail: jtappin@nso.edu

also of interest because their impact with the Earth may cause geomagnetic storms that can result in severe space weather effects such as spacecraft damage, power grid failure, and hazardous flying conditions. Physically, CMEs are density enhancements of coronal plasma that have frozen-in magnetic fields and are of size that may span several tens of degrees of heliospheric latitude and have masses that may exceed 10^{13} kg. Early in their evolution out to 0.1 – 0.2 AU they may achieve speeds greater than 3000 km s^{-1}.

CMEs and their interplanetary counterparts, known as ICMEs (Zhao, 1992; Dryer, 1994), have been observed with coronagraphs and interplanetary scintillation since the 1970s but those detected were few and far between (*e.g.*, Howard *et al.*, 1982; Hewish, Tappin, and Gapper, 1985). Since the launch of the *Solar and Heliospheric Observatory* (SOHO) (Domingo, Fleck, and Poland, 1995), its instruments have detected well over 10^4 CMEs, and their kinematics have been cataloged (St. Cyr *et al.*, 2000; Yashiro *et al.*, 2004). More recent instruments have also provided images of ICMEs beyond 20° elongation (*e.g.*, Tappin *et al.*, 2004; Howard *et al.*, 2006). ICMEs have also been investigated by *in situ* spacecraft that measure their internal structure along a single track as the ICME passes by the spacecraft (*e.g.*, Gosling *et al.*, 1994; Bothmer and Schwenn, 1998; Lepping *et al.*, 2001).

Until recently, the study of the three-dimensional (3-D) structure of CMEs has been limited primarily to modeling efforts, many of which use measurements of coronagraph and *in situ* data as inputs (*e.g.*, Lepping, Jones, and Burlaga, 1990; Chen, 1996; Xie, Ofman, and Lawrence, 2004). Three-dimensional measurements of CMEs directly from coronagraph data were not possible because images are limited to sky-plane projections of CMEs or a single track along an arbitrary axis of the CME structure. By using data alone, only estimates of 3-D structure were possible, based on known associations of CMEs with solar surface phenomena such as flares (*e.g.*, Harrison, 1995), prominences/filaments (*e.g.*, Cremades and Bothmer, 2004), and post-eruptive arcades (Tripathi, Bothmer, and Cremades, 2004). The first attempt at producing 3-D structures comparing CMEs and ICMEs by using data alone was published in 2007 (Howard *et al.*, 2007) but was based on a solar surface association.

In this paper we produce the first 3-D measurements of two CMEs using coronagraph data alone. Two limb CMEs that erupted in November 2007 are presented, neither of which is associated with a solar surface eruption. Using measurements of common features in three differently situated spacecraft (triangulation), we determine the geometry required to pinpoint the source of the CME. This provides us with the means to recreate the 3-D structure of each. We conclude with a summary of the physical implications of the 3-D reconstructions, including the time evolution of a CME-active region in the corona and the mechanism by which the Sun simplifies its magnetic field via CMEs.

2. Data and Events

The twin spacecraft of the *Solar Terrestrial Relations Observatory* (STEREO) (Kaiser *et al.*, 2008) were designed to observe solar phenomena from viewpoints remote from the Earth. Launched in October 2006 the spacecraft share a similar orbit about the Sun as the Earth, but at a growing angular distance from the Sun – Earth line. STEREO-A leads the Earth while STEREO-B lags, and the angular separation between each spacecraft and the Sun – Earth line grows by $\sim 22.5°$ per year. Each spacecraft contains a variety of *in situ* and radio instruments and also an imaging suite called SECCHI. SECCHI (Sun – Earth Connection Coronal and Heliospheric Investigation) (Howard *et al.*, 2008) consists of an extreme ultraviolet camera (EUVI), two coronagraphs (COR1 and COR2), and two heliospheric imagers (HI1 and HI2).

After the first year of operation, the STEREO spacecraft were at sufficient distance from each other and the Earth to allow reliable 3-D reconstructions of CMEs to be made by using the coronagraphs. We report on the first reconstructions of two CMEs that were observed by STEREO and SOHO on 14 – 19 November 2007. Through a process of triangulating carefully chosen measurements of the CME as observed by all three spacecraft we have demonstrated a means to reproduce the 3-D structure of each.

The two events we analyzed were "classical" three-part CMEs (leading edge, followed by a cavity, then a filament) of apparent width of around 40°. The first had an approximate onset time of 14:00 UT on 14 November 2007 and the second of 06:00 UT on 16 November 2007. In between the two events on 15 November 2007 was an Earth-directed CME (which we have not considered in the present study) and no other significant CMEs were observed during that week. Both CMEs were directed toward the southwest of the Sun relative to SOHO and both STEREO spacecraft. During this time the STEREO spacecraft were near the ecliptic plane, each $\sim 20°$ away from the Sun – Earth line and $\sim 40°$ away from each other. The instrument aboard SOHO in which both CMEs were observed is the Large Angle Spectroscopic Coronagraph (LASCO) (Brueckner *et al.*, 1995).

3. Results

3.1. Observations

The first thing to note is the appearance of the CMEs relative to each spacecraft. Figure 1 shows the first CME as observed by LASCO C2 ($2 – 6\ R_\odot$) and C3 ($3.7 – 30\ R_\odot$), the COR2s ($2 – 15\ R_\odot$), HI1-B ($\sim 12 – 85\ R_\odot$), and HI2-B ($\sim 68 – 216\ R_\odot$). Neither event was observed by the HI instruments on STEREO-A because the fields of view of these instruments are exclusively to the east. It cannot be denied that it is the same CME observed in all instruments but the appearance is slightly different for each spacecraft. For example, the CME in COR2-A appears wider (with a relative position angle range $\Delta\text{PA} \sim 57°$) than in COR2-B ($\Delta\text{PA} \sim 39°$). It also appears closer to the Sun at the same time in COR2-A than in COR2-B. These differences are the result of projection effects and imply that the first CME is closer to the sky plane relative to STEREO-B than STEREO-A. Projection effects are also greater in LASCO ($\Delta\text{PA} \sim 45°$) than in STEREO-B, but not greater than in STEREO-A. So, from inspection alone, we may reasonably conclude that this CME is closest to the sky plane relative to STEREO-B and is thus closer to the observer relative to SOHO (and the Earth) and STEREO-A.

We may likewise conduct a similar inspection of the second CME. Figure 2 shows this CME as observed by LASCO, the COR1s ($1.1 – 3\ R_\odot$) and the COR2s. Here the relative width of the CME is greater in COR2-B ($\Delta\text{PA} \sim 54°$) and LASCO ($\Delta\text{PA} \sim 46°$) than in COR2-A ($\Delta\text{PA} \sim 36°$), implying that this CME is closer to the plane of the sky of STEREO-A than the other two spacecraft. This implies that the second CME is behind the sky plane relative to SOHO and STEREO-B. This is evidenced further by the fact that the second CME is only faintly visible in HI1-B and is not detected by HI2-B (not shown). This is probably because by the time the CME has reached these distances it is too far away from the spacecraft to be easily detected.

3.2. Geometry: Triangulation

Quantitatively, we may apply appropriate geometry to measurements of the CMEs to triangulate their source. We consider three measurements for each CME: the central PA and the

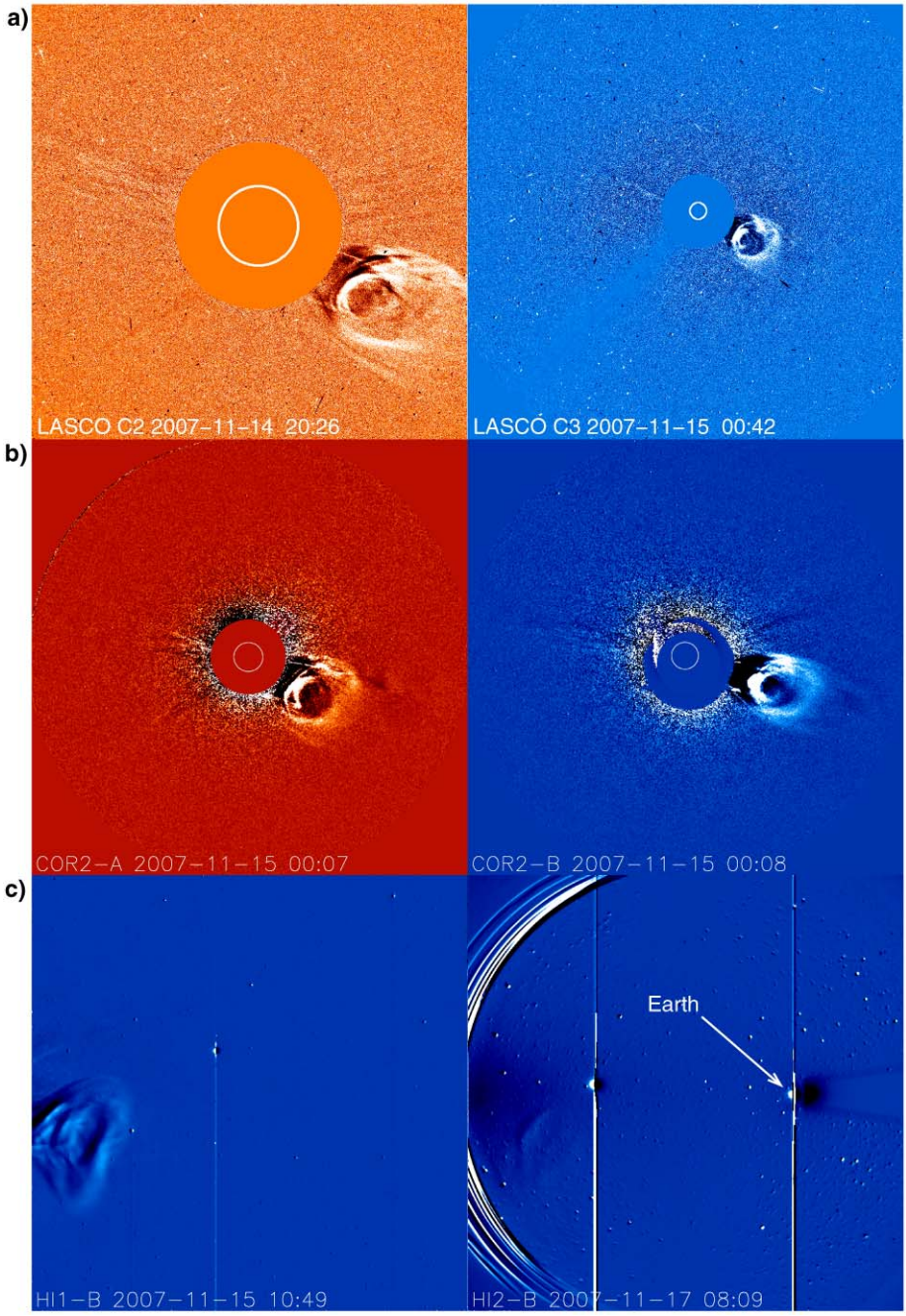

Figure 1 (a) LASCO C2 and C3, (b) STEREO COR2-A and COR2-B, and (c) STEREO HI1-B and HI2-B images of the first event. For (a) and (b) the circle at the center of the image represents the occulting disk and the white circle represents the surface of the Sun. For (c) the Sun is to the left of each image and the location of the Earth in the right panel is indicated. For each image the instrument, date, and time are labeled.

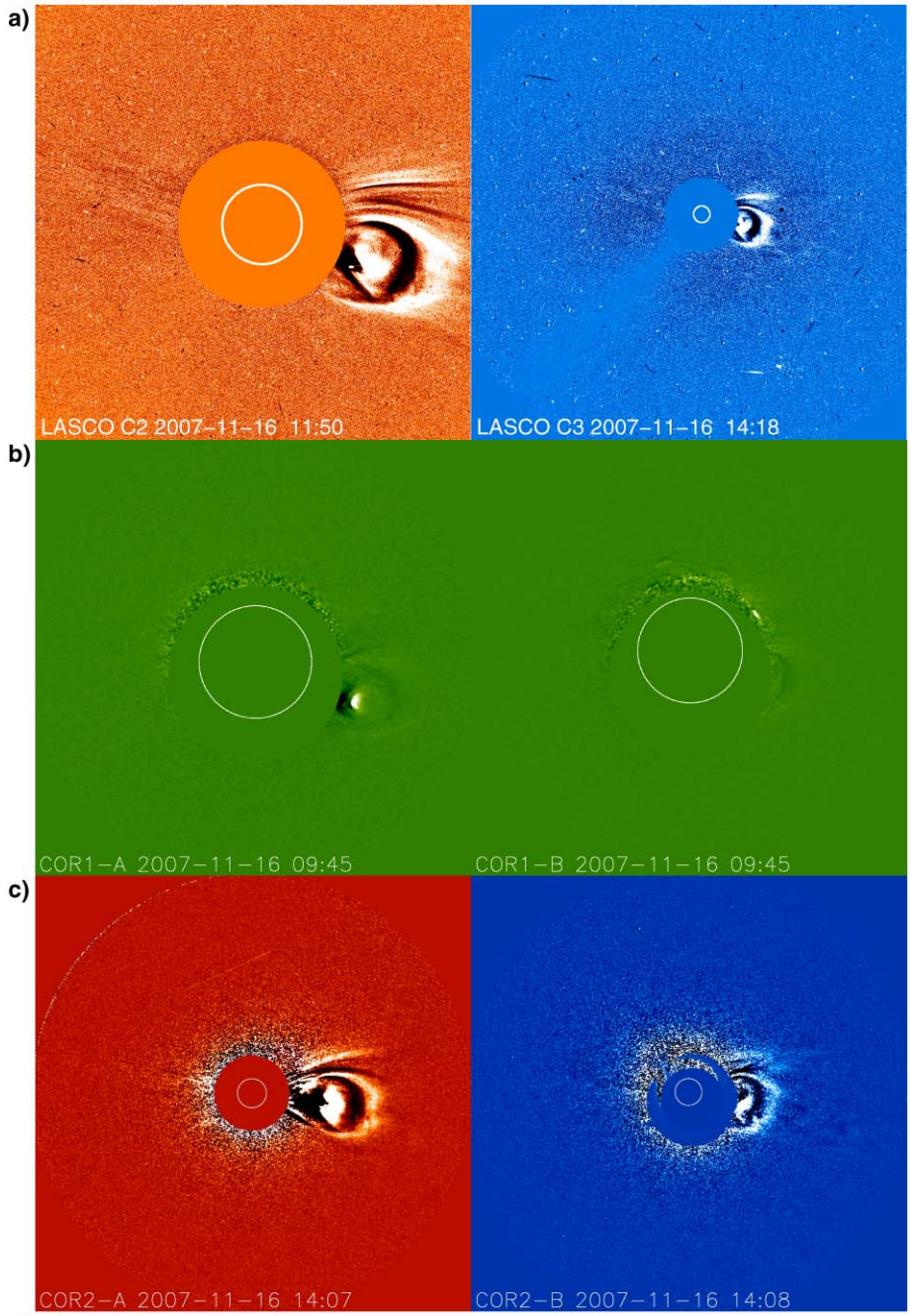

Figure 2 (a) LASCO C2 and C3, (b) STEREO COR1-A and COR1-B, and (c) STEREO COR2-A and COR2-B images of the second event.

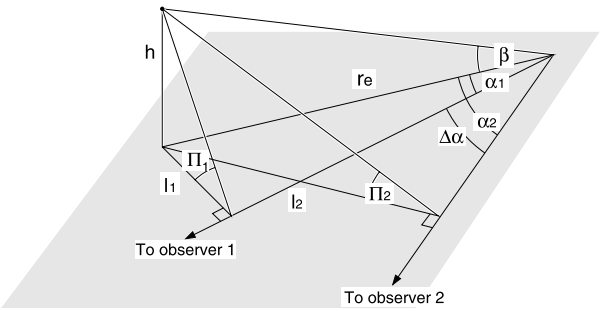

Figure 3 The geometry for determination of the 3-D location of each CME.

PA of the northern and southern flanks. Figure 3 shows the geometry of the situation. Let β be the elevation (or latitude) of the observed point from the Sun and α be the angular separation between the projection into the equatorial plane of each observer. For simplicity we have assumed that all three spacecraft are coplanar, in the ecliptic equatorial plane. There is hence a single β and three values of α to be determined, but each is separated by a known quantity $\Delta\alpha$, which is equal to the separation angle between the spacecraft. Π is hence the PA of the measured point relative to the observer. The projected distance of the point in the equatorial plane is r_e and l_1 and l_2 are the perpendicular distances from the projected point and the vectors from the Sun to observers 1 and 2, respectively.

From this geometry, it can be shown that

$$\tan\beta = \tan\Pi_1 \sin\alpha_1 = \tan\Pi_2 \sin(\alpha_1 + \Delta\alpha), \tag{1}$$

or

$$\tan\alpha_1 = \frac{\sin\Delta\alpha}{\frac{\tan\Pi_1}{\tan\Pi_2} - \cos\Delta\alpha}. \tag{2}$$

Table 1 shows the result of the three measurements (central PA and northern and southern flanks). It is necessary to rotate each into solar ecliptic coordinates and then to heliocentric coordinates by using

$$\beta' = \sin^{-1}\big(\cos\beta \sin\delta \cos(\alpha - \eta) + \sin\beta \cos\delta\big) \tag{3}$$

and

$$\alpha' = \tan^{-1}\left(\frac{\sin\beta - \sin\beta' \cos\delta}{\cos\beta \sin(\alpha - \eta)\sin\delta}\right) - \big(90^\circ - \eta\big), \tag{4}$$

where δ is the tilt of the solar axis and η is the longitude of the plane containing the solar axis and the ecliptic pole, relative to the spacecraft.

The Carrington longitudes of the northern flank, central measurement, and southern flank are shown in Table 2. Here the accuracy of the latter two measurements is clearly shown, with only a discrepancy of 1° for the central measurement and 7° for the southern flank. The northern flank is far less accurate, with discrepancies exceeding 100°. This is because the northern flank measurements were near the equator, as were both spacecraft. Discrepancies between measurements coplanar to the observers using this technique are discussed in the next section. Note that the Carrington longitudes of the central measurement for the two events are only 10° apart.

Table 1 (a) Position angle measurements of the central location (PA_c) and northern (PA_n) and southern (PA_s) flanks of each CME, compared among LASCO, COR2-A, and COR2-B. The angular separation $\Delta\alpha$ is also shown. The values in brackets represent the amount by which the position angle is rotated to align them with the ecliptic plane (so that each spacecraft is in the same plane). (b) The resultant latitude Λ and longitude Φ relative to each spacecraft in ecliptic (ec) and heliocentric (sol) coordinates.

(a)	Event 1	PA_c	PA_n	PA_s	$\Delta\alpha$
	LASCO	242.5 (−7.0)°	263.0 (−7.0)°	218.0 (−7.0)°	L-B = +20.1°
	COR2-A	233.0 (−7.5)°	261.3 (−7.5)°	204.0 (−7.5)°	A-B = +40.3°
	COR2-B	245.0 (−6.0)°	265.5 (−6.0)°	226.8 (−6.0)°	A-L = +20.2°
	Event 2				
	LASCO	255.5 (−7.0)°	279.0 (−7.0)°	233.0 (−7.0)°	B-L = −20.1°
	COR2-A	252.0 (−7.5)°	269.6 (−7.5)°	234.0 (−7.5)°	B-A = −40.3°
	COR2-B	255.5 (−6.0)°	283.0 (−6.0)°	223.0 (−6.0)°	L-A = −20.2°
(b)	Event 1	Λ_{ec} (n−c−s)	Φ_{ec} (n−c−s)	Λ_{sol} (n−c−s)	Φ_{sol} (n−c−s)
	LASCO	(11−30−44)°S	(59−57−36)°W	(6−25−42)°S	(59−60−43)°W
	STEREO-A	(12−30−45)°S	(48−36−17)°W	(11−30−47)°S	(49−40−24)°W
	STEREO-B	(10−30−44)°S	(70−78−56)°W	(3−23−38)°S	(70−79−59)°W
	Event 2				
	LASCO	(1−21−42)°S	(101−72−112)°W	(6N−14−35)°S	(102−73 − 111)°W
	STEREO-A	(1−21−43)°S	(162−52−88)°W	(5N−19−38)°S	(163−54 − 92)°W
	STEREO-B	(2−21−41)°S	(83−92−138)°W	(5N−13−37)°S	(85−92 − 138)°W

Table 2 Carrington coordinates of the northern flank, central measurement, and southern flank for each event. Values in brackets are relative to LASCO (L), STEREO-A (A), and STEREO-B (B), respectively.

	Event 1 (L, A, B)	Event 2 (L, A, B)
Northern flank	(286, 296, 277)°	(307, 28, 270)°
Central measurement	(287, 287, 286)°	(278, 279, 277)°
Southern flank	(270, 271, 266)°	(316, 317, 323)°

4. Discussion

From the results in Table 1, we can confirm the following:

1. The solar longitudes of the CMEs are roughly 20° different when measured between STEREO-A and LASCO and between LASCO and STEREO-B.
2. The first event is entirely front-sided relative to all three spacecraft, whereas the second event is partially back-sided relative to all three, mostly relative to STEREO-B.
3. There is little variation in the latitude from spacecraft to spacecraft.
4. The largest variance is for the northernmost flank, which is near the equator.
5. The Carrington longitudes of the central PA of the two CMEs are very close to each other, implying that the central PAs of these CMEs are very near the same location on the Sun. The location of the southern flank, however, differs by $\sim 50°$ between the events.

The variation near the equator is a consequence of the geometry, as each spacecraft is also near the equator. In this region the values of Π (and hence $\tan\Pi$) are small, so small errors in the measurement of Π result in large errors in the calculation of the location. This is not a problem for the measurements of the center of the CME or the southern flank of each.

Measurement of the central PA, however, poses other problems, owing to the difficulty in precisely identifying this location.

The source location of the CME can be further verified by using the height – time profiles of each CME. Distance measurements of CMEs are determined from the elongation of an individual measurement, which is the angle between the Sun – observer line and the point – observer line. This is converted to distance by using a number of assumptions appropriate for measurements close to the Sun (Howard *et al.*, 2007). However, as all CME measurements are sky-plane projected, so too are the distance measurements. As a result, speed measurements of CMEs are typically lower than their true values. Also, when viewed from different angles, different speeds are measured for the same CME. The larger the measured speed from any given point, the closer that point is to the relative plane of the sky of the instrument. These effects are demonstrated in Howard, Nandy, and Koepke (2008).

Figure 4(a) shows elongation – time plots for the central point on each CME as measured by LASCO and the CORs. By using the standard assumptions of converting elongation to distance with coronagraphs (Howard *et al.*, 2007), each elongation can be converted to a projected distance, and the gradient of the height – time plot is the speed. The respective height – time plots of each CME are shown in Figure 4(b). Note that the larger the projection effects, the lower the projected speed, and the speed values confirm the claims made so far about the relative location of the CMEs. Finally, we can convert the elongation values into a true 3-D distance using the source location of the central PA and some simple geometry (Howard *et al.*, 2007). The 3-D distances and resulting speeds are shown in Figure 4(c). There is an improvement to the three speeds, and the distance values have a lower variance for both events. For the 3-D corrections we have used the location of the southern flank in each case, based on the larger uncertainty in the measurements of both the northern flank and the central point. This verifies the source location and provides for the first time a true 3-D speed for CMEs determined solely from coronagraph data.

With the source location verified, we may provide the means for a 3-D reconstruction of the CME. Figure 5 shows the two CMEs from two perspectives: the solar surface projection (panel (a)) and down (southward) onto the ecliptic plane (panel (b)). Note that the three points are further apart for the northern flanks and one point for Event 2 is a large distance from the others. This is because of the large errors associated with coplanar measurements, as already discussed. These events were chosen because there is no significant solar surface activity of any kind associated with these events, and so this triangulation method is the only way in which the direction of these CMEs could be even estimated.

5. Conclusions

The physical implications of this new method are fourfold:

1. The central location of the CME (and northern flank, according to our assumption) for the second event is 13° to the west of the first, whereas the southern flank is 68° to the west. Given that the Sun has rotated $\sim 26°$ to the west during the 48 hours between the launch of the two CMEs it is likely that the same coronal magnetic source was responsible for both CMEs. This is confirmed in the Carrington longitude measurements.
2. The difference between the 3-D structure of the two CMEs (signified by the reversal in direction between the two flanks, where the southern flank lies to the east of the central measurement for Event 1, but to the west for Event 2) suggests that a major reconfiguration of the coronal magnetic field must have taken place between the eruptions of the CMEs. It is possible (but unlikely) that the Earth-directed CME that was launched between these two may have played a role in this magnetic reconfiguration.

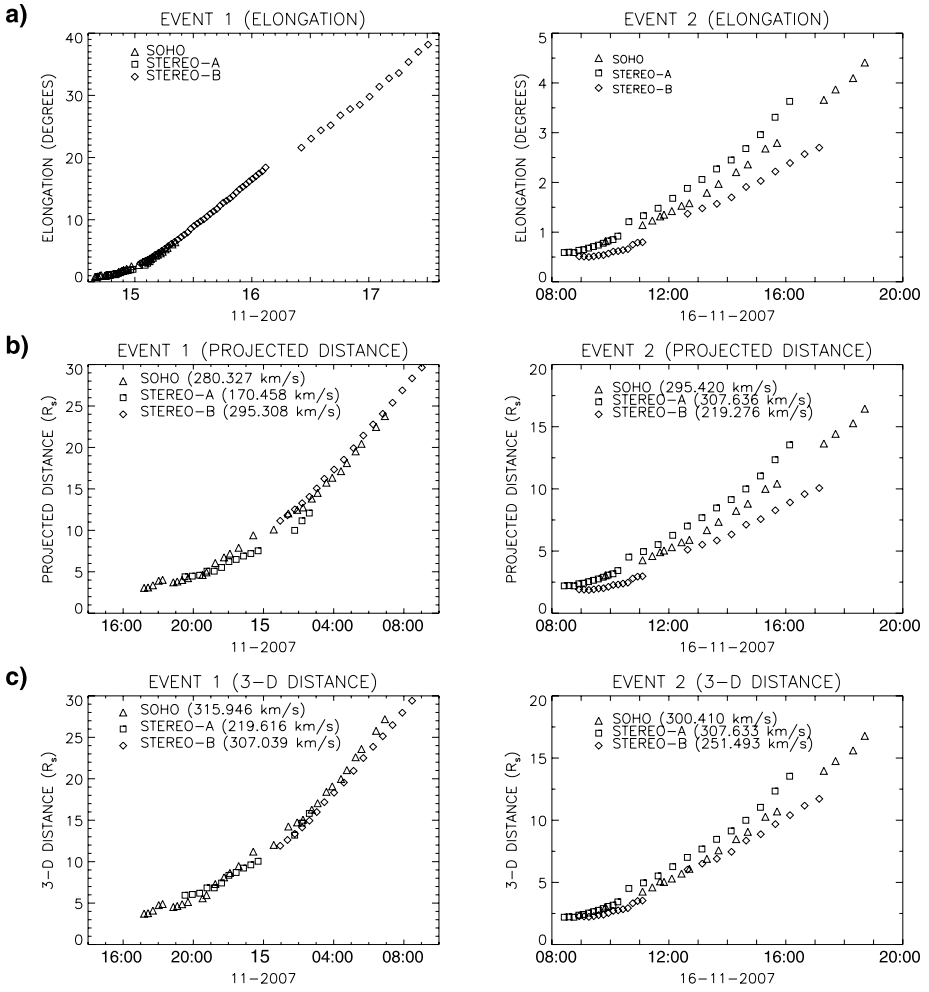

Figure 4 (a) Elongation – time plots for each event, including the HI data for the first event and the COR1 data for the second. (b) Projected distance versus time plots for each event. (c) Corrected 3-D distance for each event, using the geometry from Figure 3. For parts (b) and (c) the speed relative to each spacecraft is shown.

3. The instability in the magnetic field that caused the eruption of the two CMEs did not translate in any detectable way to the lower solar atmosphere. This suggests that the outer layers of coronal magnetic structures may erupt as CMEs while leaving the inner coronal magnetic structure intact (Howard and Harrison, 2004).
4. If the previous point is correct, then the underlying magnetic structure responsible for the first CME may also be responsible for the second, since the remnants of the original structure still remain. Perhaps the Sun is often unable to dispose of the complexity of a magnetic structure in a single eruption, and so it must remove it in sections, manifested by the eruption of multiple CMEs from the same location in relatively quick succession.

To conclude, we have demonstrated one major function for which STEREO was intended – the study of 3-D structures from the Sun. We have shown for the first time how

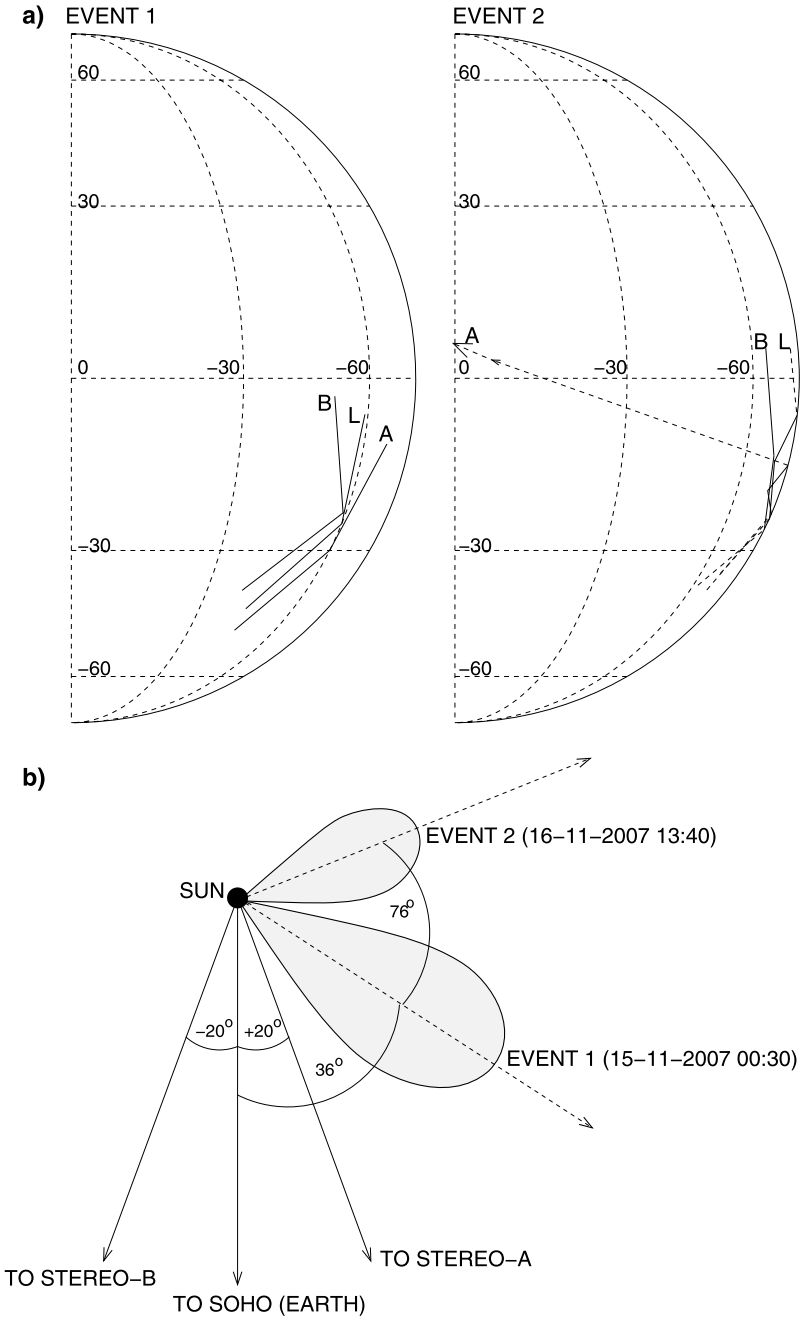

Figure 5 The 3-D recreation of each CME. (a) The location of the CME projected onto the solar surface for (left) Event 1 and (right) Event 2, with solar latitude and longitude contours added. The three traces on each disk represents the projected location from all three spacecraft, rotated into the SOHO field of view. Dashed lines for Event 2 represent measurements behind the solar limb. (b) Each CME as viewed down onto the equatorial plane from the north. The directions to each of the three spacecraft is indicated, along with the relative distance of each CME based on the times chosen (and indicated).

geometrical triangulation techniques can be applied to multiple spatially separated observatories to measure the 3-D structure of CMEs without the need for a solar surface association. We have also identified some of the problems other workers are likely to face in their own reproduction – particularly the large errors associated with coplanar (*i.e.*, ecliptic plane) measurements of the CMEs. Clearly this technique is best when measuring CMEs away from the equatorial plane. Based on the most accurate measurements of each CME and taking solar co-rotation into account, our results suggest that different parts of a large-scale magnetic structure erupt at different times. This may explain why CMEs often appear to erupt from the same region of the Sun. Perhaps the Sun is unable to dispose of all of its magnetic complexity in a given region at once, and so several eruptions are required.

Acknowledgements This work is supported in part by the National Research Council Fellowship Program, funded by AFOSR Contract No. F49620-02C-0015. The National Solar Observatory is operated by AURA, Inc., under cooperative agreement with the National Science Foundation. Partial support for NSO is provided by the USAF under a Memorandum of Agreement.

References

Bothmer, V., Schwenn, R.: 1998, *Ann. Geophys.* **16**, 1.
Brueckner, G.E., Howard, R.A., Koomen, M.J., Korendyke, C.M., Michels, D.J., Moses, J.D., Socker, D.G., Dere, K.P., Lamy, P.L., Llebaria, A., Bout, M.V., Schwenn, R., Simnett, G.M., Bedford, D.K., Eyles, C.J.: 1995, *Solar Phys.* **162**, 357.
Chen, J.: 1996, *J. Geophys. Res.* **101**, 27499.
Cremades, H., Bothmer, V.: 2004, *Astron. Astrophys.* **422**, 307.
Domingo, V., Fleck, B., Poland, A.I.: 1995, *Solar Phys.* **162**, 1.
Dryer, M.: 1994, *Space Sci. Rev.* **67**, 363.
Gosling, J.T., Bame, S.J., McComas, D.J., Phillips, J.L., Goldstein, B.E., Neugebauer, M.: 1994, *Geophys. Res. Lett.* **21**, 1109.
Harrison, R.A.: 1995, *Astron. Astrophys.* **304**, 585.
Hewish, A., Tappin, S.J., Gapper, G.R.: 1985, *Nature* **314**, 137.
Howard, T.A., Harrison, R.A.: 2004, *Solar Phys.* **291**, 315.
Howard, T.A., Nandy, D., Koepke, A.C.: 2008, *J. Geophys. Res.* **113**, A01104. doi:10.1029/2007JA012500.
Howard, R.A., Michels, D.J., Sheeley, N.R. Jr., Koomen, M.J.: 1982, *Astrophys. J.* **263**, L101.
Howard, T.A., Webb, D.F., Tappin, S.J., Mizuno, D.R., Johnston, J.C.: 2006, *J. Geophys. Res.* **111**, A04105. doi:10.1029/2005JA011349.
Howard, T.A., Fry, C.D., Johnston, J.C., Webb, D.F.: 2007, *Astrophys. J.* **667**, 610.
Howard, R.A., Moses, J.D., Vourlidas, A., Newmark, J.S., Socker, D.G., Plunkett, S.P., Korendyke, C.M., Cook, J.W., Hurley, A., Davila, J.M., Thompson, W.T., St. Cyr, O.C., Mentzell, E., Mehalick, K., Lemen, J.R., Wuelser, J.P., Duncan, D.W., Tarbell, T.D., Wolfson, C.J., Moore, A., Harrison, R.A., Waltham, N.R., Lang, J., Davis, C.J., Eyles, C.J., Mapson-Menard, H., Simnett, G.M., Halain, J.P., Defise, J.M., Mazy, E., Rochus, P., Mercier, R., Ravet, M.F., Delmotte, F., Auchere, F., Delaboudinière, J.-P., Bothmer, V., Deutsch, W., Wang, D., Rich, N., Cooper, S., Stephens, V., Maahs, G., Baugh, R., Mcmullin, D.: 2008, *Space Sci. Rev.* **136**, 67.
Kaiser, M.L., Kucera, T.A., Davila, J.M., St. Cyr, O.C., Guhathakurta, M., Christian, E.: 2008, *Space Sci. Rev.* **136**, 5.
Lepping, R.P., Jones, J.A., Burlaga, L.F.: 1990, *J. Geophys. Res.* **95**, 11957.
Lepping, R.P., Berdichevsky, D.B., Burlaga, L.F., Lazarus, A.J., Kasper, J., Desch, M.D., Wu, C.-C., Reames, D.V., Singer, H.J., Smith, C.W., Ackerson, K.L.: 2001, *Solar Phys.* **204**, 285.
St. Cyr, O.C., Howard, R.A., Sheeley, N.R. Jr., Plunkett, S.P., Michels, D.J., Paswaters, S.E., Koomen, M.J., Simnett, G.M., Thompson, B.J., Gurman, J.B., Schwenn, R., Webb, D.F., Hildner, E., Lamy, P.L.: 2000, *J. Geophys. Res.* **105**, 18169.
Tappin, S.J., Buffington, A., Cooke, M.P., Eyles, C.J., Hick, P.P., Holladay, P.E., Jackson, B.V., Johnston, J.C., Kuchar, T., Mizuno, D., Mozer, J.B., Price, S., Radick, R.R., Simnett, G.M., Sinclair, D., Waltham, N.R., Webb, D.F.: 2004, *Geophys. Res. Lett.* **31**, L02802. doi:10.1029/2003GL018766.
Tripathi, D., Bothmer, V., Cremades, H.: 2004, *Astron. Astrophys.* **422**, 337.
Xie, H., Ofman, L., Lawrence, G.: 2004, *J. Geophys. Res.* **109**, A03109. doi:10.1029/2003JA010226.
Yashiro, S., Gopalswamy, N., Michalek, G., St. Cyr, O.C., Plunkett, S.P., Howard, R.A.: 2004, *J. Geophys. Res.* **109**, A07105. doi:10.1029/2003JA010282.
Zhao, X.-P.: 1992, *J. Geophys. Res.* **97**, 15051.